Journal of Luminescence 155 (2014) 275–281

Contents lists available at ScienceDirect

Journal of Luminescence

journal homepage: www.elsevier.com/locate/jlumin

Microstructure and blueshift in optical band gap of nanocrystalline $Al_xZn_{1-x}O$ thin films

M.A. Majeed Khan [a,*], Sushil Kumar [b], M. Naziruddin Khan [a], Maqusood Ahamed [a], A.S. Al Dwayyan [a,c]

[a] King Abdullah Institute for Nanotechnology, King Saud University, Riyadh 11451, Saudi Arabia
[b] Materials ScienceLaboratory, Department of Physics, Chaudhary Devi Lal University, Sirsa 125055, India
[c] Physics and Astronomy Department, College of Science, King Saud University, P.O. Box 2455, Riyadh 11451, Saudi Arabia

ARTICLE INFO

Article history:
Received 5 March 2014
Received in revised form
3 June 2014
Accepted 5 June 2014
Available online 1 July 2014

Keywords:
Al doped ZnO thin films
Photoluminescence
Surface Morphology
Raman shift
Optical bandgap

ABSTRACT

In this paper, we report the structural and optical properties of Al doped ZnO (AZO) thin films grown on glass substrates using the sol–gel process. To understand the effect of Al doping on the structural and optical response of ZnO nanoparticles thin films, the prepared samples have been characterized using X-ray diffraction (XRD), energy dispersive spectroscopy (EDS), transmission electron microscopy (TEM), high resolution transmission electron microscopy (HRTEM), photoluminescence (PL), UV–vis absorption and Raman spectroscopy. X-ray diffraction results show that Al doped ZnO nanoparticles have hexagonal phase similar to ZnO nanoparticles. TEM images as well as XRD data exhibit the estimated size of nanoparticles to be in the range 35–45 nm. The optical band gap has been determined from optical absorption spectra. The band gap varied from 3.27 eV for undoped ZnO film to 3.87 eV for AZO film having 3 atwt% Al. The blue shift in energy band gap mainly related to carrier concentration induced by Al-donor doping, and to the degree of crystalline order. Photoluminescence study further confirms the blue shift in UV emission when Al doping concentration is increased, as a consequence of extension in band gap.

1. Introduction

Nanocrystalline materials have attracted a wide attention due to their unique properties and immense potential applications in nano devices fabrication [1,2]. New physical properties and advanced technologies both in sample preparation and device fabrication evoke on account of the development of nanoscience and nanotechnology. Zinc oxide (ZnO) is one of the versatile compound semiconductors with excellent properties and extensive applications in electronics, optoelectronics, sensors, catalysis etc. [3]. ZnO thin films have attracted considerable attention because they can be tailored to possess high electrical conductivity, high infrared reflectance and high visible transmittance using different coating techniques [4]. Some of the remarkable properties of ZnO are its wide direct band gap ~3.37 eV, and the binding energy of exciton ~60 meV, which makes it an excellent material for excitonic devices [5]. It has been recognized that a small amount of Al doping increases its electrical conductivity by more than 3 orders of magnitude at room temperature [6]. Doped ZnO, especially Al doped ZnO, is one of the best n-type thermoelectric oxide materials reported to date [7]. Several researchers [8–12] have studied the effect of doping of metals (Al^{3+}, In^{3+}, Ga^{3+} etc.) on the microstructure, electrical and optical properties of ZnO. A number of fabrication techniques such as sputtering [13], pulsed laser deposition (PLD) [14], and chemical vapor deposition (CVD) [15] have been adopted to deposit good quality Al doped ZnO (AZO) thin films. In this paper, we report on the synthesis of undoped and Al doped ZnO nanoparticles (NPs) prepared by the sol–gel process and their thin films deposited by spin coating unit; and on the study of their structural, morphological and optical properties. The structure and morphology of ZnO NPs are studied by X-ray diffraction (XRD), transmission electron microscopy (TEM) and selected area electron diffraction (SAED); while optical properties are studied using UV–vis absorption, photoluminescence and Raman scattering techniques. Through this study, we attempted to correlate the microstructure, light absorption and emitting properties of $Al_xZn_{1-x}O$ nanoparticles.

2. Experimental details

It is reported in literature [16,17] that it is possible to synthesize sol–gel ZnO samples using zinc nitrate in addition to zinc

* Corresponding author. Tel.: +966 14 67 6188; fax: +966 14 67 0662.
E-mail address: majeed_phys@rediffmail.com (M.A. Majeed Khan).

http://dx.doi.org/10.1016/j.jlumin.2014.06.007
0022-2313/

acetate. ZnO prepared with zinc nitrate exhibits nanostructured fine grains. It has been found that ZnO prepared using zinc nitrate shows a rapid and random crystallization compared to that of ZnO prepared using zinc acetate. Zinc nitrate was used as the precursor material in the present study. To prepare undoped ZnO nanoparticles, 1 M zinc nitrate hexahydrate ($Zn(NO_3)_2 \cdot 6H_2O$) was mixed with the appropriate amount of stabilizer ethylene glycol $(CH_2OH)_2$ in de-ionized water. For Al-doped ZnO (AZO) nanoparticles, aluminum nitrate nanohydrate ($Al(NO_3)_3 \cdot 9H_2O$) was added into the solution to serve as aluminum source. The amount of $Al(NO_3)_3 \cdot 9H_2O$ was controlled precisely and kept at the selected concentration of aluminum. Two Al atomic contents of 1 and 3 atwt% were chosen, then stirred in clear solution at 70 °C for 1 h. Meanwhile, citric acid ($C_6H_8O_7$) was dropped into these solutions slowly until the solutions had a uniform distribution and became transparent (pH∼2). The solutions were then aged for 48 h to assure that the chemical process was completed. After ageing, some portion of solutions was stored separately for thin film deposition process, while the remaining portion of solutions were placed in an oven at 110 °C until the solvent evaporated; and then the dried samples were grinded into fine powders using pestle and mortar. Undoped and Al-doped ZnO thin films were deposited by spin coating technique. The glass substrates were cleaned using organic solvents and ultrasonic agitator. The coating solutions were dropped onto the substrates, which were rotated at 3500 rpm for 1 min. After spin coating, the films were dried at 110 °C to evaporate the solvent and to remove organic residuals. The coating and drying processes were repeated 5 times to increase thin film thickness. The deposition process was conducted for all prepared solutions to obtain thin films of different Al-contents. Finally, thin films as well as nanopowders were put into a muffle furnace to perform heat treatment at 700 °C for 3 h. The structural characteristics of prepared undoped and Al doped ZnO nanopowders/thin films were examined using X-ray diffraction (XRD, PANalytical X'Pert) with CuK_α radiation (λ=0.154 nm) operated at 45 kV and 40 mA, field emission transmission electron microscopy (FE-TEM, JEM-2100F, JEOL), high resolution transmission electron microscopy (HRTEM), selected area electron diffraction (SAED) and Raman spectroscopy. The energy dispersive spectroscopy (EDS) was performed for the compositional analysis of samples. The micro-PL and micro-Raman scattering were carried out using a Raman/PL system (JY-Horiba-T64000) in conjunction with a He–Cd Kimmon continuous wave laser operating at a wavelength of 325 nm (3.8 eV) as the excitation source. The UV–vis analysis was carried out in the wavelength range of 190–1100 nm using a double beam UV–vis–NIR spectrophotometer (Thermo scientific evolution 60 S) with a resolution of 0.5 nm.

3. Results and discussion

3.1. XRD

The crystal structure of undoped and Al doped ZnO thin films has been determined using X-ray diffraction data (Fig. 1). XRD analysis shows that all the prepared samples can be indexed to hexagonal wurtzite structure (JCPDS 89-0510) and are independent of alumina content. It presents the corresponding zinc oxide peaks only, which indicates that the doping of Al ions does not change the wurtzite structure of ZnO [18] and exhibits the formation of single phase $Al_xZn_{1-x}O$ nanoparticles. It has been observed that the broadening of diffraction peaks increases with increase in Al doping, which confirms the decrease in the crystallinity and the particle size of the prepared material [19]. As the

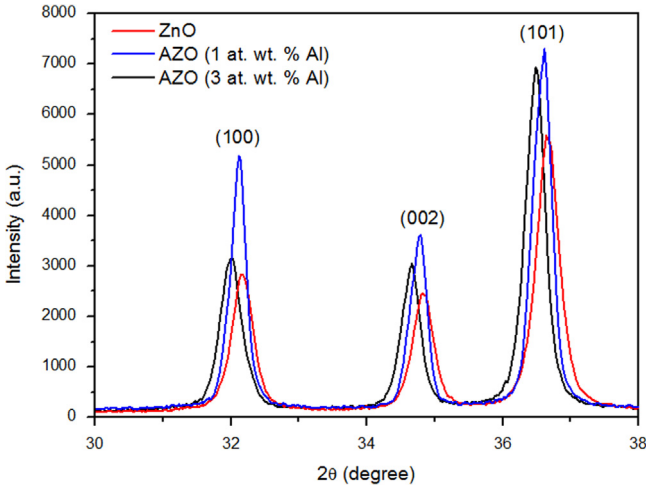

Fig. 1. XRD patterns of undoped and Al-doped (1 and 3 at%) ZnO nanoparticles thin films.

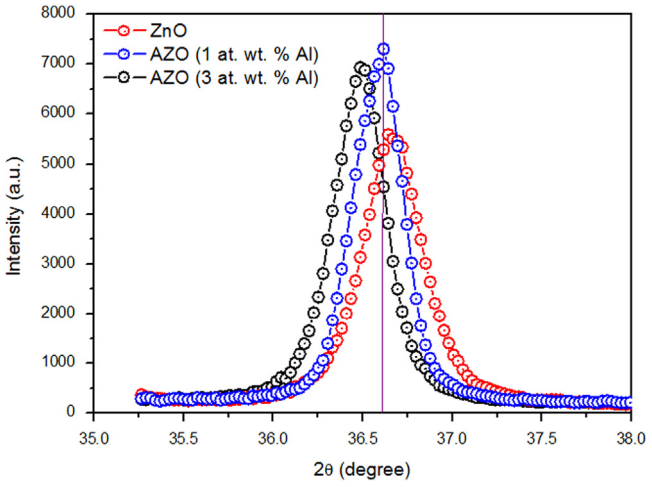

Fig. 2. XRD patterns (zoom) corresponding to (1 0 1) peak of undoped and Al-doped (1 and 3 at%) ZnO nanoparticles thin films.

Al content is increased, the peaks corresponding to (1 0 0), (0 0 2) and (1 0 1) planes shifted slightly to lower angles (Fig. 1).

The crystallite size (D) has been calculated using Scherrer relation;

$$D = \frac{0.9\lambda}{\beta \cos \theta} \quad (1)$$

where β is FWHM of a peak, θ is the angle of diffraction and λ is the wavelength of incident X-rays. Crystallite size of each sample has been calculated corresponding to most intense peak (1 0 1) of prepared nanoparticles (Fig. 2) and are tabulated in Table 1. The lattice parameters have been calculated using the relation [20]:

$$\frac{1}{d^2_{hkl}} = \frac{4}{3}\left(\frac{h^2+hk+k^2}{a^2}\right) + \frac{l^2}{c^2} \quad (2)$$

where h,k,l are Miller indices, a and c are lattice constants, and d_{hkl} is inter-planer spacing. The mean values of lattice constants a=0.3252 nm and c=0.5207 nm, are in accordance with the previously reported results [20,21]. The decrease in crystallite size with the increase of dopant is probably because of the substitution

Table 1
Microstructural and optical properties of Al doped ZnO thin films.

Samples	Crystallite size (nm) (From XRD)	Crystallite size (nm) (From TEM)	Dislocation density (δ) (nm^{-2})	Micro-strain (ε)	No. of crystallites/ volume (N)	Stacking fault probability (γ)	Band gap E_g (eV)
ZnO	43.3	44	5.41×10^{-4}	2.52×10^{-3}	183.88	12.965	3.27
$Al_1Zn_{99}O$	38.7	41	6.93×10^{-4}	1.87×10^{-3}	235.46	12.947	3.69
$Al_3Zn_{97}O$	35.2	38	8.16×10^{-4}	1.20×10^{-3}	277.55	12.923	3.87

of larger radius Zn^{2+} (0.074 nm) by the smaller radius Al^{3+} (0.05 nm) at the lattice points of ZnO nanocrystal [18].

Further, the dislocation density (δ), the micro-strain (ε) and the numbers of crystallites per unit volume (N) have been estimated using following relations [22–24]:

$$\delta = \frac{1}{D^2} \tag{3}$$

$$\varepsilon = \frac{\lambda}{D\cos\theta} - \frac{\beta}{\tan\theta} \tag{4}$$

$$N = \frac{d}{D^2} \tag{5}$$

where D is the crystallite size, λ is the wavelength of incident X-rays, β is FWHM of a peak and d is the thickness of film. The estimated parameters are reported in Table 1.

The stacking fault probability γ is the fraction of layers undergoing stacking sequence faults in a given crystal and hence one fault is expected to be found in $1/\gamma$ layers. The presence of stacking faults gives rise to shifts in the peak positions of different reflections with respect to standard position in a fault free sample. Three typical experimental profiles showing the peak shift for hexagonal (1 0 1) reflection of ZnO film with respect to Al doped ZnO thin films are shown in Fig. 2. The peak shift is mainly due to the increasing Al content and the decreasing crystallite size.

The relation connecting stacking fault probability (γ) with peak shift $\Delta(2\theta)$ is given by [25]

$$\gamma = \frac{2\pi^2}{45\sqrt{3}} \frac{\Delta(2\theta)}{\tan\theta_{101}} \tag{6}$$

where $\Delta(2\theta)$ is the shift in peak position and θ_{101} is the angle of diffraction corresponding to (1 0 1) peak. From above Eq. (6), the stacking fault probability has been calculated by measuring the peak shift with doping of Al in ZnO. The values of microstrain and stacking fault probability of undoped and Al doped ZnO are reported in Table 1. It is seen that Al doping in ZnO induces low microstrain and low stacking fault probability improving the stoichiometry of films and causing the volumetric expansion of thin films.

The morphology of undoped and Al doped ZnO nanoparticles has been investigated by field emission transmission electron micrographs (FETEM) shown in Figs. 3(a) and (b) respectively, which reveal that as-grown NPs are almost spherical in shape with average particle size in the range 35–45 nm. The self generated elemental composition details are presented in EDS pattern shown in Figs. 4(a) and (b). The additional peaks assigned to C and Cu are due to the carbon coated copper grid used in electron microscopy. It is clear from these figures that Zn and O are the main elemental species in pure ZnO sample while additional Al peaks are observed in Al doped samples. Crystallinity and preferential orientation of nanoparticles in the samples are confirmed from selected area electron diffraction (SAED) patterns shown in Figs. 5(a) and (b). The SAED pattern obtained by focusing the beam on a few nanoparticles of the sample clearly indicates the single crystalline nature of nanoparticles. It also confirms that the nanoparticles are

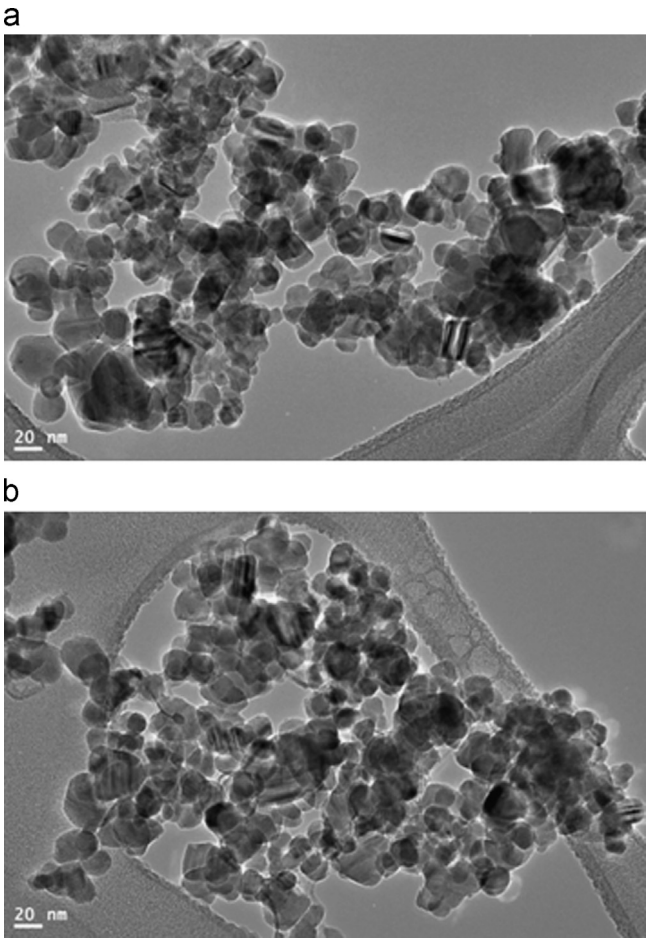

Fig. 3. TEM micrographs of undoped (a) and Al-doped (3 at%) (b) ZnO nanoparticles.

indeed in the wurtzite phase. Further, HRTEM study has been applied to analyze the lattice fringes for undoped and doped samples, which are presented in Figs. 6(a) and (b) respectively. From these figures, one can see that no sign of segregation of impurity could be detected, indicating that the grain is single crystalline and free from secondary crystalline phases. In addition, the d-spacing of crystal planes is calculated as 0.243 nm and 0.253 nm for undoped and 3 atwt% Al doped ZnO samples respectively, indicating the preferable crystal growth along (1 0 1) plane and it is the most intense peak in XRD pattern shown in Fig. 1.

3.2. Raman spectroscopy

Raman spectroscopy is an important non-destructive technique for estimating the crystallinity and studying the vibrational properties of nanomaterials such as ZnO. In our case, Raman scattering is used to clarify the quality and the structure of prepared samples. Fig. 7 shows the Raman spectra of prepared nanoparticles excited by 514 nm line of argon laser. All samples

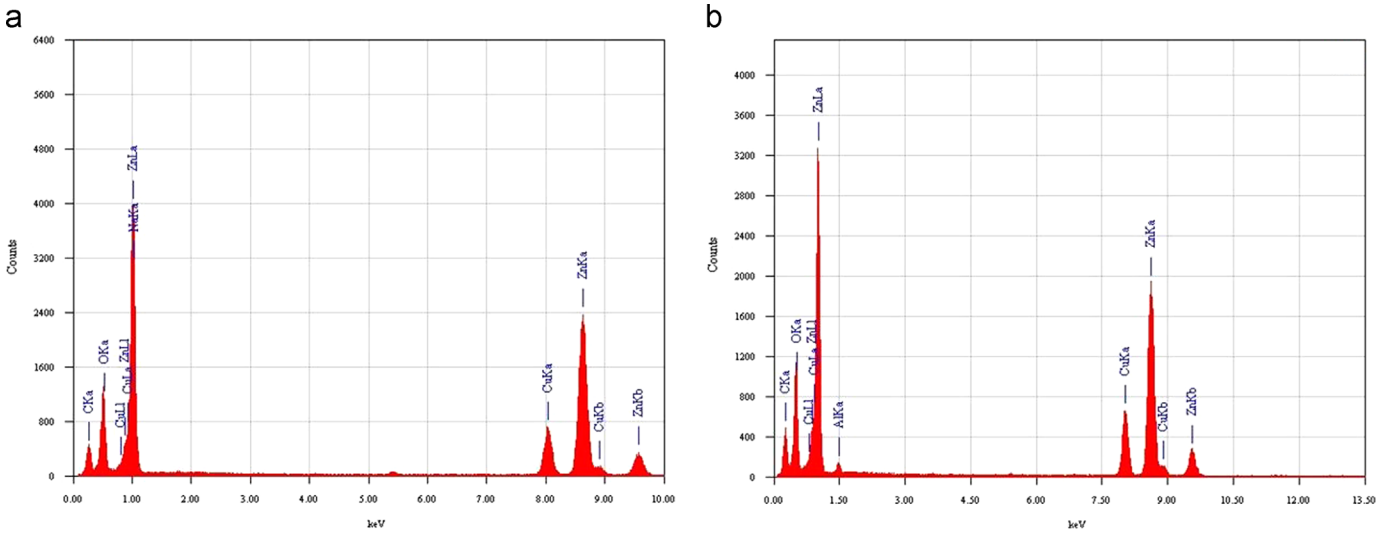

Fig. 4. EDS spectra of undoped (a) and Al-doped (3 at%) (b) ZnO nanoparticles.

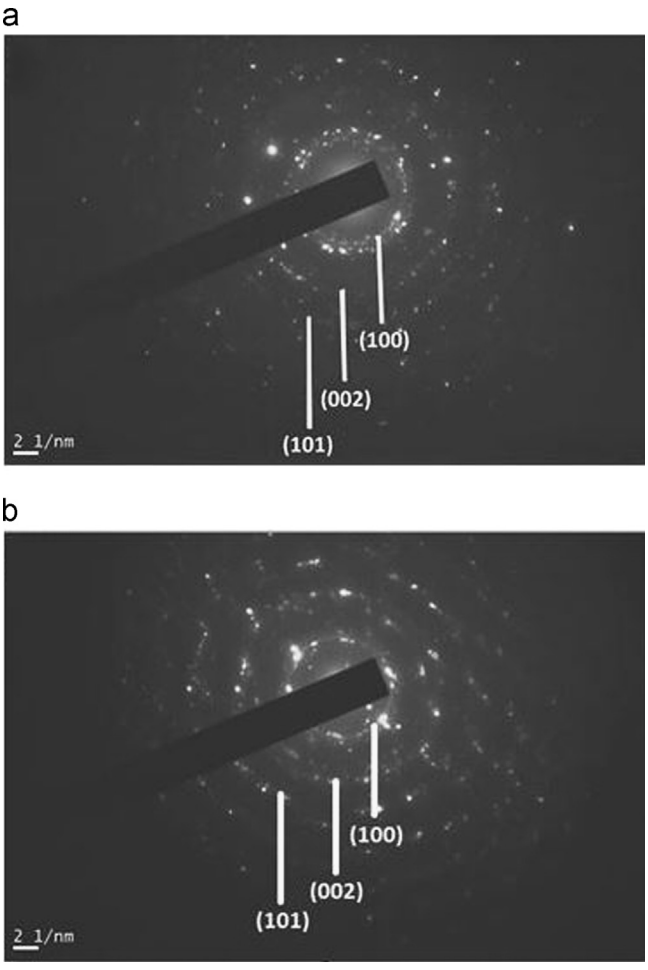

Fig. 5. SAED patterns of undoped (a) and Al-doped (3 at%) (b) ZnO nanoparticles.

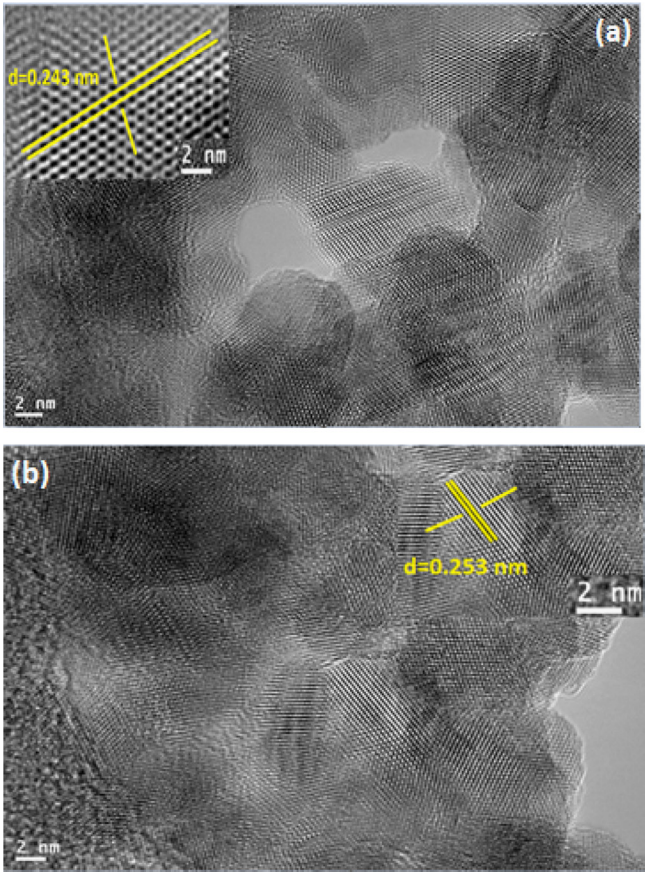

Fig. 6. HRTEM images of undoped (a) and Al-doped (3 at%) (b) ZnO nanoparticles.

represent an obvious band at 369 cm^{-1} corresponding to a second-order Raman scattering process, which has been proved to be $E_2^{high}-E_2^{low}$ difference mode [26]. This band is also related to second order Raman process as described by some researchers and is assigned to $2E_2^{low}$ mode which needs further confirmation [27,28].

In addition, Raman spectra of undoped and Al doped (1, 3 atwt%) ZnO nanoparticles present other vibrational bands at 1409, 1376 and 1365 cm^{-1} respectively, which may be attributed to nth order ($n=1, 2, 3$) A1 (LO) phonons. The position of peak (A_{1L} and E_{1L}) varies from 1376 to 1365 cm^{-1} for Al doped ZnO nanoparticles, and that of undoped one is about 1409 cm^{-1}. It can be seen that the position of A_{1L} and E_{1L} peak shift to lower wave number as compared to undoped ZnO, which may be due to point defects such as oxygen vacancies or zinc interstitials [29,30]. It may also be due to the fact that the addition of Al may change the free

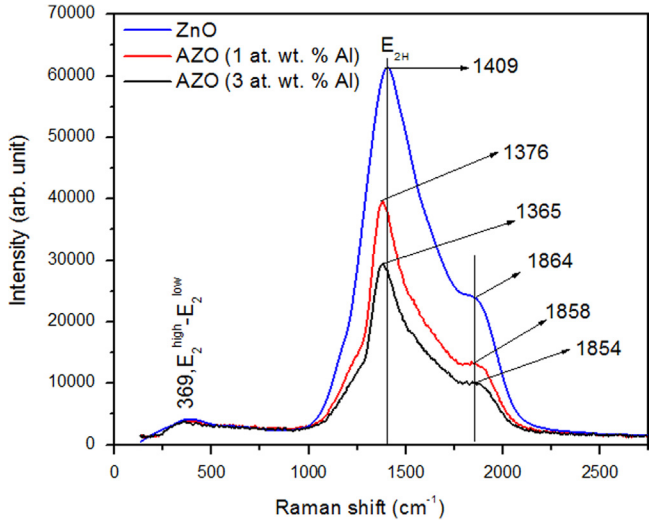

Fig. 7. Raman spectra of undoped and Al-doped (1 and 3 at%) ZnO nanoparticles.

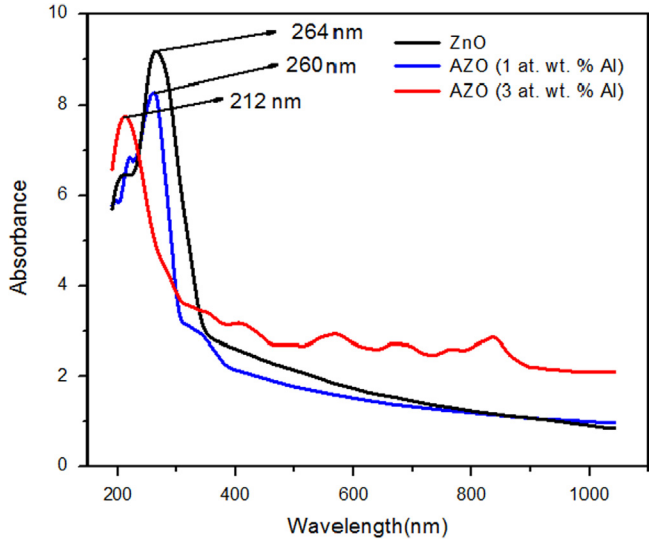

Fig. 8. UV-visible absorbance spectra of undoped and Al-doped (1 and 3 at%) ZnO nanoparticles thin films.

carrier concentration in ZnO nanoparticles. In addition, the peaks centered at ~1864, 1858 and 1854 cm^{-1}, in undoped and Al doped (1, 3 atwt %) ZnO nanoparticles respectively, corresponds to 3LO multiphonon scattering [31]. The E_2 modes correspond to characteristic band of wurtzite phase. The appearance of LO phonon peak has been attributed to the formation of oxygen defects, interstitial zinc, and free carrier. According to Fig. 7, the E_{2H} peak shows a dominant intensity over the LO phonon peak and have a very sharp feature. It indicates that the wurtzite structure is formed, and ZnO and ZnO:Al crystals are of good quality, which is in agreement with XRD result. The broad feature of LO phonon peaks, especially 2LO phonon modes, can be ascribed to the defect electronic states within the band gap existing in samples.

3.3. Optical absorption

To study the optical quality of undoped and Al doped ZnO nanoparticles thin films, optical absorption investigations have been carried out. The optical absorbance spectra of prepared nanoparticles are shown in Fig. 8. A strong absorption peak appears at 264 nm for undoped ZnO, which is significantly blue shifted corresponding to bulk ZnO (370 nm). The size reduction of Al doped ZnO samples may be owing to smaller ionic radius of Al compared to ionic radius of Zn. In addition, blue shift in absorption of undoped and doped samples reveals an increase in band gap which is probably due to the quantum size effect.

In the following discussion, we mainly focus on the optical properties of $Al_xZn_{1-x}O$ films with 0–3 atwt% Al content. The fundamental absorption, which corresponds to electron excitation from valence to conduction band, is usually employed to determine the value of optical band gap (E_g). As a direct band gap semiconductor, ZnO, has an absorption coefficient (α) obeying the following relation for high photon energies ($h\nu$):

$$(\alpha h\nu)^2 = A(h\nu - E_g) \tag{7}$$

The absorption coefficient α may be defined as

$$\alpha = \frac{x}{d} \tag{8}$$

where A is a constant, ν is the photon frequency, d is the thickness of film and x is the absorbance.

The optical band gap values are determined from Eq. (7) by plotting the square of optical absorption coefficient as a function of photon energy and by extrapolating the linear region to the energy axis (Fig. 9). The obtained values are 3.27 eV for undoped film; and 3.69 and 3.87 eV for 1 and 3 atwt% Al doped ZnO films respectively. Blue shift due to Al doping has been largely attributed to the Burnstein–Moss effect [32]. The donor Al atoms provide additional carriers which cause the Fermi level to move into the conduction band, so that the energy gap becomes larger. Moreover, ZnO is a natural n-type material and the Fermi level would move into the conduction band when it is doped with Al. Since the states below Fermi level in the conduction band are filled, the absorption edge should shift towards higher energy. If the Fermi level indeed shifts into the conduction band, the Al doped ZnO should reveals metallic characteristics as that of Sn doped indium oxide [33]. Recently, Imai et al. [34] have determined the electronic band structure of undoped and doped ZnO using density functional theory under the local density approximation. They found that the shape of the density of states curve and the band structure of undoped and doped ZnO are similar to each other, i.e., a semiconductor-to-metal transition does not occur in this system

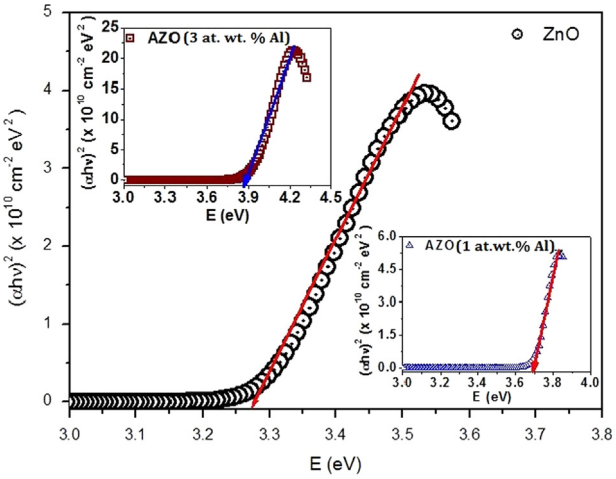

Fig. 9. $(\alpha h\nu)^2$ vs photon energy plots of the corresponding samples used to determine their optical band gaps.

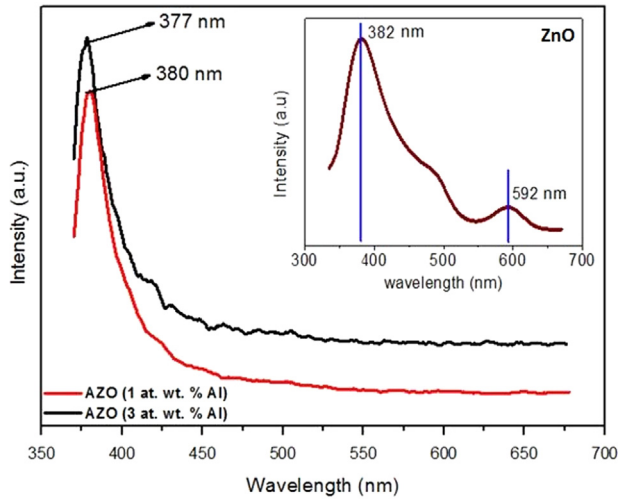

Fig. 10. Photoluminescence spectra of undoped and Al-doped (1 and 3 at%) ZnO nanoparticles thin films at room temperature under the excitation of 330 nm laser beam.

with increasing Al doping concentration. Experimentally, Gabás et al. [35] have measured the valence-band structure of undoped ZnO and Al doped (1 and 3 atwt%) ZnO films, but they found that no samples reveal any density of states around the Fermi level. Hence the Fermi level of Al doped ZnO does not locate inside the conduction band. Physically, the band gap growth in Al doped ZnO system may originate from the change in the nature and in the strength of interaction potentials between the donors and the host crystals.

3.4. PL spectroscopy

Photoluminescence (PL) study has been performed to check the optical quality and the possible effects of Al doping in ZnO. Fig. 10 shows the room temperature PL spectra of undoped and Al doped ZnO samples under the excitation of 330 nm laser beam. Undoped ZnO shows two emission peaks: one at 382 nm (UV emission peak) corresponds to near band edge emission of ZnO and another at 592 nm (visible emission) relates to the transition between the electrons close to the conduction band and the holes at vacancies associated with the surface defects [36]. After Al doping, the UV emission peak position of AZO nanoparticles exhibited a slight blue-shift from 380 nm (3.26 eV) to 377 nm (3.29 eV), and the intensity is increased with increasing Al concentration, which is attributed to an increase in non-radiative recombination. For the blue emission of ZnO material, although some related results have been reported, but the emission mechanism of blue light is still unclear. Some research groups found that undoped ZnO thin films have blue emission [37,38], while others found that doped ZnO thin films have blue emission [39,40]. This indicates that the blue emission is concerned with both native point defects such as Zn interstitials and Zn vacancies, and doped impurities. So far, several blue emission mechanisms have been proposed, there are three main viewpoints as follows: (a) the electron transition from Zn interstitial levels to the top of valence band [41–44]; (b) the electron transition from V_0 to valence band [45]; (c) the electron transition from the bottom of conduction band to Zn vacancy levels [39,46]. The sharp UV emission peak around 3.29 eV presumably results from excitons. Due to the large exciton binding energy of ZnO (about 60 meV), excitons have been observed at room temperature. It has also been reported that thermal energy at room temperature may be enough to release bound excitons because the binding energy of bound exciton is only a few meV [47]. The exciton level of our samples occurred at 3.29 eV, and is blue shifted with respect to the typical reported free exciton peak at 3.26 eV [48]. These PL results are in good agreement with XRD results.

4. Conclusions

The structure, morphology and optical properties of sol–gel derived nanoparticles have been investigated. The samples have hexagonal wurtzite structure and are highly crystalline in nature. The average particle size has been found in the range 35–45 nm. TEM, HRTEM and SAED measurements confirmed that prepared samples are nanocrystalline; and the particle sizes are in good agreement with those determined from XRD. UV–vis absorption spectra show a relatively narrow absorption band at 264 nm which is blue shifted with that of bulk. The optical absorption increases with increase in Al doping, and leads to an increase in optical band gap. PL spectra of prepared nanoparticles show a strong UV emission band located at 382 nm due to near band-edge emission. The shift of optical band gap, the quenching of near-band-edge photoluminescence, and the enhancement of LO modes multi-phonon resonant Raman scattering in ZnO:Al crystals may be attributed to the incorporation of Al in ZnO. The results indicate that the tuning of optical band gap and photoluminescence can be achieved by controlling the Al concentration in $Al_xZn_{1-x}O$ nanocrystalline films. The prepared samples have potential applications in the fabrication of light emitting devices.

Acknowledgments

The authors are grateful to the King Abdullah Institute for Nanotechnology, for financially supporting this work. Author M.A. Majeed Khan is thankful to J. Puzon Labis (KAIN) for kind help in TEM experiments.

References

[1] X. Wang, J. Song, J. Liu, Z.L. Wang, Science 316 (2007) 102.
[2] K. Keren, R.S. Berman, E. Buchstab, U. Sivan, E. Braun, Science 302 (2003) 1380.
[3] S. Das, S. Chaudhuri, Appl. Surf. Sci. 253 (2007) 8661.
[4] Y.R. Ryu, S. Zhu, J.D. Budai, H.R. Chandrasekhar, P.F. Miceli, H.W. White, J. Appl. Phys 88 (2000) 201.
[5] L. Wang, N.C. Giles, J. Appl. Phys. 94 (2003) 973.
[6] M. Ohtaki, T. Tsubota, K. Eguchi, H. Arai, J. Appl. Phys. 79 (1996) 1816.
[7] H. Cheng, X.J. Xu, H.H. Hng, J. Am. Ceram. Int. 35 (2009) 3067.
[8] H.M. Zhou, D.Q. Yi, Z.M. Yu, L.R. Xiao, J. Li, Thin Solid Films 515 (2007) 6909.
[9] G. Srinivasan, R.T. Rajendra Kumar, J. Kumar, Opt. Mater. 30 (2007) 314.
[10] E.J.L. Arredondo, A. Maldonado, R. Asomoza, D.R. Acosta, M.A.M. Lira, M. de la, L. Olvera, Thin Solid Films 490 (2005) 132.
[11] V. Fathollahi, M.M. Amini, Mater. Lett. 50 (2001) 235.
[12] K.J. Chen, T.H. Fang, F.Y. Hung, L.W. Ji, S.J. Chang, S.J. Young, Y.J. Hsiao, Appl. Surf. Sci. 254 (2008) 5791.
[13] T. Minami, H. Nanto, S. Takata, Jpn. J. Appl. Phys. 23 (1984) L280.
[14] F.K. Shan, G.X. Liu, W.J. Lee, B.C. Shin, J. Appl. Phys. 101 (2007) 053106.
[15] W.S. Lau, S.J. Fonash, J. Electron. Mater. 16 (1987) 141.
[16] H. Bahadur, S.B. Samanta, A.K. Srivastava, K.N. Sood, R. Kishore, R.K. Sharma, A.B. Rashmi, M. Kar, P. Pal, V. Bhatt, S. Chandra, J. Mater. Sci. 41 (2006) 7562.
[17] H. Bahadur, A.K. Srivastava, R.K. Sharma, S. Chandra, Nanoscale Res. Lett. 2 (2007) 469.
[18] Z. Jin, Q. WenXiu, Y. Yuan, Z. Peng, L. YuLong, Sci. China Phys. Mech. Astron 55 (2012) 1198.
[19] S. Hartner, M. Ali, C. Schulz, M. Winterer, H. Wiggers, Nanotechnol 20 (2009) 1.
[20] A. Drici, G. Djeteli, G. Tchangbedji, H. Derouiche, K. Jondo, K. Napo, J.C. Bernède, S. Ouro-Djobo, M. Gbagba, Phys. Status Solidi (A) 201 (2004) 1528.
[21] Su-Shia Lin, Jow-Lay Huang, P. Sajgalik, Surf. Coat. Technol. 185 (2004) 254.
[22] A.I. Borhan, A.R. Iordan, M.N. Palamaru, Mater. Res. Bull. 48 (2013) 2549.
[23] R. Sathyamoorthy, S. Chandramohan, P. Sudhagar, D. Kanjilal, D. Kabiraj, K. Ashokan, Sol. Energy Mater. Sol. Cells 90 (2006) 2297.
[24] S. Gopal, C. Viswanathan, B. Karunagaran, S.a.K. Narayandass, D. Mangalaraj, J. Yi, Cryst. Res. Technol. 40 (6) (2005) 557.
[25] V. Potin, P. Ruterana, G. Nouet, J. Phys. C: Condens. Matter 12 (2000) 10301.

[26] R. Cusco, E. Alarcon-Llado, J. Ibanez, L. Artus, J. Jimenez, B. Wang, M.J. Callahan, Phys. Rev. B 75 (2007) 165202.
[27] K.A. Alim, V.A. Fonoberov, M. Shamsa, A.A. Balandin, J. Appl. Phys. 97 (2005) 124313.
[28] P.K. Samanta, S.K. Patra, A. Ghosh, P. RoyChaudhuri, Int. J. Nanosci. Nanotechnol. 1 (2009) 81.
[29] Y. Huang, M. Liu, Z. Li, Y. Zeng, S. Liu., Mater. Sci. Eng. B 97 (2003) 111.
[30] W. Da, S. Wu, K. Liu, W. Chen, S. Pan, Chin. J. Light Scatt. 18 (2006) 43.
[31] B. Kumar, H. Gong, S.Y. Chow, S. Tripathy, Y. Hua, Appl. Phys. Lett. 89 (2006) 071922.
[32] E. Burstein, Phys. Rev 25 (1982) 7826.
[33] Z.Q. Li, J.J. Lin, J. Appl. Phys. 96 (2004) 5918.
[34] Y. Imai, A. Watanabe, I. Shimono, J. Mater. Sci.: Mater. Electron. 14 (2003) 149.
[35] M. Gabás, S. Gota, J.R. Ramos-Barrado, M. Sánchez, N.T. Barrett, J. Avila, M. Sacchi, Appl. Phys. Lett. 86 (2005) 042104.
[36] A.V. Dijken, E.A. Meulenkamp, D. Vanmaekelbergh, A. Meijerink, J. Phys. Chem. B 104 (2000) 1715.
[37] C. Wang, D. Xu, X. Xiao, Y. Zhang, D. Zhang, J. Mater. Sci. 42 (2007) 9795.
[38] Z.J. Yan, D.W. Zeng, C.S. Xie, H.H. Wang, W.L. Song, Thin Solid Films 517 (2009) 1541.
[39] H. Xue, X.L. Xu, Y. Chen, G.H. Zhang, S.Y. Ma, Appl. Surf. Sci. 255 (2008) 1806.
[40] A. Wang, B. Zhang, X. Wang, N. Yao, Z. Gao, Y. Ma, L. Zhang, H. Ma, J. Phys. D: Appl. Phys 41 (2008) 215308.
[41] H.X. Chen, J.J. Ding, X.G. Zhao, S.Y. Ma, Physica B 405 (2010) 1339.
[42] H. Zeng, G. Duan, Y. Li, S. Yang, X. Xu, W. Cai, Adv. Funct. Mater. 20 (2010) 561.
[43] X. Peng, H. Zang, Z. Wang, J. Xu, Y. Wang, J. Lumin. 128 (2008) 328.
[44] H. Zeng, W. Cai, Y. Li, J. Hu, P. Liu, J. Phys. Chem. B 109 (2005) 18260.
[45] Y. Hu, Y.Q. Chen, Y.C. Wu, M.J. Wang, G.J. Fang, C.Q. He, S.J. Wang, Appl. Surf. Sci 255 (2009) 9279.
[46] Y.Y. Peng, T.E. Hsieh, C.H. Hsu, Nanotechnology 17 (2006) 174.
[47] Y. Chen, D.M. Bagnall, H.J. Koh, K.T. Park, K. Hiraga, Z. Zhu, T. Yao, J. Appl. Phys. 84 (1998) 3912.
[48] P. Zu, Z.K. Tang, G.K.L. Wong, M. Kawasaki, A. Ohtomo, H. Koinuma, Y. Segawa, Solid State Commun. 103 (1997) 459.